Volume Measurement Technology of Dispensing Transparent Adhesives Based on Line Laser Scanning

Ling Cao*
College of Electronics and Information Engineering, Shenzhen University,
Department of R&D
OPT Machine Vision
Dongguan, China
caoling@optmv.com

Renjie Zhou*
Guangdong Polytechnic Normal University
Guangzhou, China
Department of R&D
OPT Machine Vision
Dongguan, China
1053013397@qq.com
*co-first author

Xinhua Wang
Guangdong Polytechnic Normal University
Guangzhou, China
wangxh@gpnu.edu.cn

Wei Pan**
Department of R&D
OPT Machine Vision
Dongguan, China
vpan@foxmail.com
**Corresponding author

***Abstract*—Accurate volume measurement of transparent adhesives is essential for controlling the dispensing process, calibrating adhesive discharge, and enhancing both product quality and manufacturing efficiency. We introduced a complementary spectral background optimization (CSBO) method to enhance three-dimensional (3D) reconstruction accuracy by attenuating transmitted light, thereby reducing internal scattering and reflection interference without requiring additional measurement tools or equipment. In addition, we proposed an improved gray-scale center of gravity extraction algorithm by utilizing a unique candidate points mechanism and the novel dynamic weighted multi-factor scoring constraints (DWMF-SC) method for effectively candidate points screening. The proposed method was experimentally validated through various experiments. The experimental results demonstrate that the proposed laser center line extraction method outperforms traditional methods with higher precision and robust anti-interference properties, while the CSBO approach achieved the lowest relative error ratio reaching about 1.40% compared to ground truth values.**

Keywords—3D reconstruction, volume measurement, laser scanning, transparent object measurement, 3d metrology

I. INTRODUCTION

Conventional pneumatic dispensers regulate adhesive deposition through air pressure magnitude and valve actuation duration. However, inherent system limitations, particularly fluctuations in air pressure, pose significant challenges to maintaining uniform adhesive discharge. Excessive material deposition may induce adhesive overflow, while insufficient discharge risks causing inadequate bonding strength or compromised airtightness. These issues ultimately lead to product performance failures and quality deterioration. Consequently, the precise volume measurement of dispensed adhesive serves as a critical process control node, providing essential data-driven guidance for calibration of adhesive discharge, with direct implications for enhanced product quality and manufacturing efficiency.

Traditional optical 3D measurement methods demonstrate significant limitations when applied to transparent adhesives [1], and typically exhibit substantial measurement inaccuracies or even fail to achieve complete reconstruction. This study designed a volume measurement system for transparent adhesives to address the challenges. The proposed system utilizes a line laser scanning system [2] to acquire higher precision transparent adhesives depth map data. Furthermore, multi-stage 3D reconstruction and geometry analysis algorithms are employed to achieve high precision measurements of transparent adhesives volume.

II. IMAGING OPTIMIZATION METHOD AND SYSTEM COMPOSITION

A. Complementary spectral background optimization

As shown in Fig. 1, the proposed CSBO method employs a dispensing nozzle to extrude transparent adhesives onto the green-yellow substrate with green-yellow spectral absorption characteristics [3], which serves as background panels for specimen preparation and experimental design. The underlying principle exploits wavelength-selective absorption, where materials exhibit wavelength-dependent optical interactions through preferential absorption of specific spectral bands while transmitting or reflecting others. This quantum mechanical phenomenon is governed by discrete energy states inherent to atomic systems, wherein electron transitions to elevated energy states occur through resonant photon absorption when incident photon energy corresponds to the inter-state energy differential [4]. The expression for photon energy E and the inter-state energy differential ΔE is as follows:

$$E = h * f = \frac{h*c}{\lambda} \tag{1}$$

$$\Delta E = E_{excited\ state} - E_{ground\ state} = \frac{h*c}{\lambda_{absorbed}} \tag{2}$$

Where λ is wavelength of absorbed light, f denotes the optical frequency, h represents Planck's constant, and c corresponds to the speed of light, $\lambda_{absorbed}$ is wavelength of absorbed light. Consequently, material-specific energy level differences induce wavelength-selective photon absorption, thereby generating distinctive complementary absorption of spectral features through quantum state transitions. The relation

between matter's color and color absorbed is shown in Tab. 1. The violet laser employed in the 3D sensor demonstrates spectral complementarity with green-yellow substrate. This optical method effectively attenuates complementary transmitted laser through green-yellow substrate, thereby suppressing scattering artifacts and specular reflection interference, as depicted in Fig. 2.

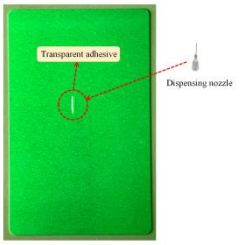

Fig. 1. Schematic of designed transparent adhesives specimen.

TABLE I. THE RELATION BETWEEN MATTER'S COLOR AND COLOR ABSORBED

Light Absorbed			Perceived Complementary (Subtraction) Color	
Wavelength(nm)	Color			
400-435	Violet		Green-yellow	
435-480	Blue		Yellow	
480-490	Green-blue		Orange	
490-500	Blue-green(cyan)		Red	
500-560	Green		Purple(magenta)	
560-580	Yellow-green		Violet	
580-595	Yellow		Blue	
595-605	Orange		Green-blue	
605-650	Redorange		Blue-green(cyan)	
650-750	Red		Green	

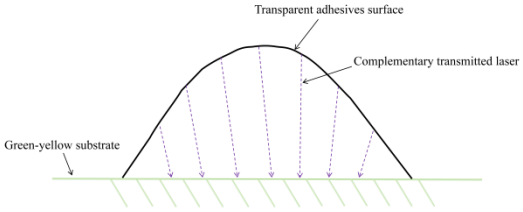

Fig. 2. Schematic of complementary transmitted laser absorbed by green-yellow substrate.

B. *Imaging system composition*

The 3D line laser scanning system is shown in Fig. 3. Designed specimen is mounted on a mobile robotic platform, where a calibrated 3D line laser scanning camera projects violet laser stripe onto the transparent adhesives dispensing region. Through synchronized image data acquisition during planar scanning trajectories, surface data of the transparent adhesives specimen are obtained.

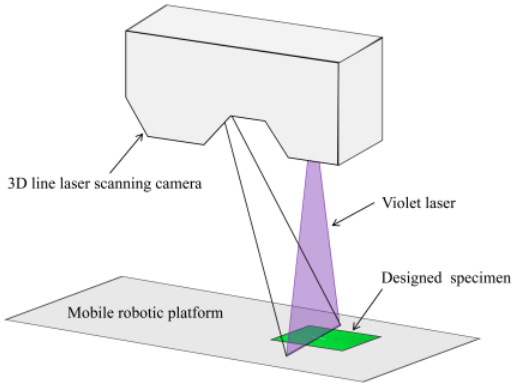

Fig. 3. Schematic of 3D line laser scanning system.

III. METHOD FOR 3D RECONSTRUCTION

The procedure after acquiring surface data is divided into three steps: extraction of candidate points, post-processing of candidate points, depth map reconstruction. The role of each step is as follows:

1) The initial phase involves filtering out random noise through input image filter preprocessing. Subsequently, directional-consistency-verified gradient analysis is integrated with the gray-scale center of gravity extraction algorithm to extract the set of candidate center points.

2) The proposed DWMF-SC method conducts the preliminary screening of candidate points.

3) In the final stage, all center lines are integrated into a depth map space to reconstruct the 3D surface of the transparent adhesives.

A. *Extraction of candidate points*

In order to mitigate interference from random noise, image smoothing is implemented in the image set through mean filtering. After that, each image in the image set is extracted separately for directional-consistency-verified gradient analysis to locate laser stripe candidate regions on a per-pixel-row basis. The schematic of candidate regions localization is shown in Fig. 4. Based on the differences in grayscale value between neighboring pixels, this method is employed to validate candidate regions, with the specific principle described as follows:

$$\left.\begin{array}{l}\left.\begin{array}{l} I_b - I_a \geq K \\ I_c - I_b \geq 0 \end{array}\right\} \rightarrow \mathrm{I}_{\,\mathrm{Rising}} \in [a,c] \\ \left.\begin{array}{l} I_c - I_d \geq 0 \\ I_d - I_e \geq K \end{array}\right\} \rightarrow \mathrm{I}_{\,\mathrm{Falling}} \in [c,e] \end{array}\right\} \rightarrow \mathrm{I} \in [b,d] \quad (3)$$

Here, I_a, I_b, I_c, I_d, I_e is the grayscale value of the points a, b, c, d, e. K denotes the edge detection gradient threshold, which can control the region edge. Consequently, the region $\mathrm{I}_{\,\mathrm{Rising}}$ and $\mathrm{I}_{\,\mathrm{Falling}}$ is categorized as gray-scale rising delay and gray-scale falling delay. Synthesizing the two parts delay leads to candidate region $\mathrm{I} \in [b,d]$ excluding the two endpoints. Analogously, candidate regions II and III are determined. Within each candidate region, candidate center

Identify applicable funding agency here. If none, delete this text box.

points are calculated through gray-scale center of gravity extraction method [5]. Assuming the column value range of candidate region is $x \in [x_s, x_c]$ in a row, the conventional formula for gray-scale center of gravity extraction algorithm is as follows:

$$x_{center} = \frac{\sum_{x=x_s}^{x_c} w(I_x) * x}{\sum_{x=x_s}^{x_c} w(I_x)} \tag{4}$$

$$w(I_x) = \frac{I_x}{256 - I_x} \tag{5}$$

Where, I_x is the grayscale value of point x, x_{center} represents the column coordinate value of candidate center point. $w(I_x)$ denotes grayscale density weighting model to highlight salient features within target area and improve localization accuracy. Finally, the positions of initial candidate points are extracted from each pixel row for the whole map.

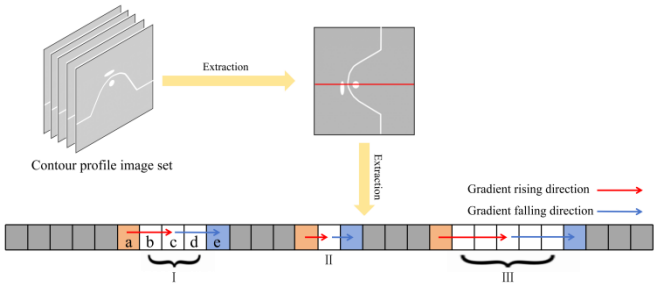

Fig. 4. Schematic of candidate regions localization.

B. Post-processing of candidate points

Based on the extracted candidate points, we proposed the DWMF-SC method for preliminary screening of candidate points. The specific steps of this method are described below.

1) The first step is to analyze the continuity of the candidate points by searching for the neighboring preceding and subsequent rows. Position offset constraint is expressed using the following formula:

$$|x_c^{(k)} - x_{neighbor}| \leq zValue \tag{6}$$

Where, $x_c^{(k)}$ represents column value at the *k-th* point form candidate point set c in a row, $x_{neighbor}$ denotes the column value at the adjacent point form the preceding and subsequent row of *k-th* point, $zValue$ indicates the maximum position offset threshold. Then, the normalized continuity score can be deduced:

$$S_{continuity}^{(k)} = \frac{L^{(k)}}{max(L)} \tag{7}$$

Here, $L^{(k)}$ is the number of points that satisfy predefined position offset constraint at *k-th* point. $max(L)$ represents the maximum L among point set c.

2) Furthermore, grayscale intensity score of *k-th* point can be determined as:

$$S_{intensity}^{(k)} = \frac{I^{(k)}}{I_{max}} \tag{8}$$

Where, $I^{(k)}$ is the grayscale value of *k-th* point, I_{max} is the maximum grayscale value among point set c. In the third part, historical position score of *k-th* point is shown in the following formula:

$$S_{history}^{(k)} = 1 - \frac{|x_c^{(k)} - x_{prev}|}{R} \tag{9}$$

Here, x_{prev} denotes column value at the initial screened point in the preceding row of *k-th* point, R is the normalization factor that can be expressed as the total number of columns or the maximum x_{prev} among point set c.

3) After calculating the scores of the above three parts, the multi-factor dynamic weighted model was used to calculate the final score of *k-th* point:

$$\begin{cases} S_{final}^{(k)} = \alpha * S_{continuity}^{(k)} + \beta * S_{intensity}^{(k)} + \gamma * S_{history}^{(k)} \\ I^{(k)} < 0.1 * I_{max} \\ w > 20 \end{cases} \rightarrow S_{final}^{(k)} = 0 \tag{10}$$

Where, $\alpha = 0.5$, $\beta = 0.1$, $\gamma = 0.4$ is the score weighting factor, w is the candidate region pixel width. For excluding invalid points, the points are filtered out both with grayscale value less than 10% of I_{max} among point set c and w larger than 20 pixel bits. The unique point in each row is obtained by calculating the maximum final score among point set c.

C. Depth map reconstruction

The depth map [6] data space is a two-dimensional matrix containing depth *Z-values* and *X* and *Y* direction coordinate information. As shown in Fig. 5, the spatial aggregation of all center lines is projected into a depth map space according to its spatial distribution characteristics. Therefore, spatial coordinates in *X*, *Y* and *Z* axes are recorded in the true distance pixel units to generate the 3D surface depth map of the reconstructed transparent adhesives.

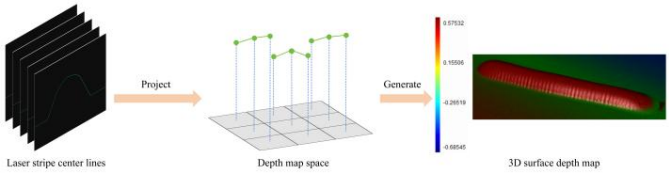

Fig. 5. Schematic of transparent adhesives 3D surface depth map reconstruction.

IV. Geometry Analysis

A. Plane fitting and rectification

Prior to volume measurement, the measurement workflow initiates with defining a datum plane for the measured specimen to determine the optimal spatial distribution of depth map data for subsequent coordinate system unification. As depicted in Fig. 6, the general process of the method is as follows:

1) With the yellow region of interest (ROI) designated a s the target domain in the figure, obtaining randomly sampled

regions of the platform depth map data serves as the local plan e fitting data.

2) The plane fitting algorithm [7] based on principal component analysis (PCA) is used to fit the ROI depth map data. The equation of the datum plane can be express as:$ax + by + cz + d = 0$, where *a*, *b*, *c*, and *d* are the fitted plane model parameters.

3) After plane fitting computation, rigid-body transform ation [8] is implemented to perform rotation and translation op erations on the original depth map data.

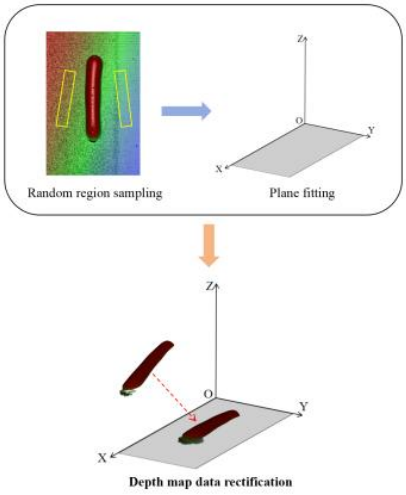

Fig. 6. Schematic of plane fitting and rectification.

B. Connectivity-based segmentation

This step performs connectivity-based segmentation [10] on the depth map, as shown in Fig. 7(a), to segment the background and isolate volume measurement regions specific to the transparent adhesives. This segmentation method first applies 3D Otsu thresholding algorithm to generate a binarized image, and then traverses the image based on run-length encoding (RLE) . Subsequently, it allocates regions across the entire image through eight-neighborhood connectivity analysis on encoded sequences, iterating until all connected regions are identified. Finally, geometric filtration is applied to extract the green connected domain representing convex depth features that exceed predefined depth threshold, as depicted in Fig. 7(b).

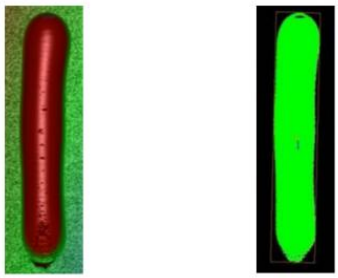

Fig. 7. (a) Transparent adhesives depth map; (b) The result of connectivity-based segmentation method.

C. Volume calculation

Ultimately, as illustrated in Fig. 8, the segmented adhesive volume measurement region undergoes geometric decomposition where each pixel is regarded as an independent rectangular prism through the projection integration method [9]. The base dimensions of each prism correspond to the image's spatial resolution $\Delta x \times \Delta y$, while the height is defined by depth values z_{xy} from the calibrated depth map. The total adhesive volume is then calculated through volumetric integration of all individual prisms, expressed as:

$$V = (\Delta x * \Delta y) * \sum_{(x,y)\in R} z_{xy} \tag{11}$$

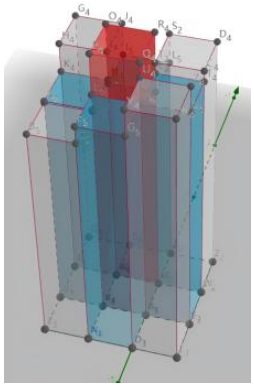

Fig. 8. Schematic of projection integration volume algorithm.

V. Experiment and Result Analysis

A. Experimental setup

To validate the effectiveness and feasibility of the proposed method, we conducted various experiments on the experimental system. The system consists of two modules: an image acquisition and imaging module, and an image processing and control module. As shown in Fig. 9, the image acquisition and imaging module is composed of a 3D line laser scanning camera with mobile robotic platform and test specimen. After image acquisition, the algorithm is implemented by a program written in C++ executed on the image processing and control module (a standard PC platform).

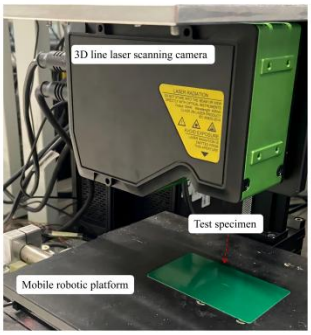

Fig. 9. The composition of image acquisition and imaging module.

B. *Experiments and comparisons of laser center line extraction*

Comparative experiments were conducted between the proposed algorithm and other traditional algorithms, including the Steger, gray-scale center of gravity, thinning algorithm. To verify the robustness and stability of the proposed algorithm, experiment was performed on an image with significant surface roughness and edge diffusion noise as shown in Fig. 10. From the image, we can see that the profile of the laser stripe is uneven. Additionally, due to the metallic luster of the object's material, there are many edge diffusion noises in the image, which greatly affects the extraction of the center line of the laser stripe. This type of interference is commonly found in many metallic components. The extraction results of the proposed algorithm and other traditional algorithms in this image are shown in Fig. 11.

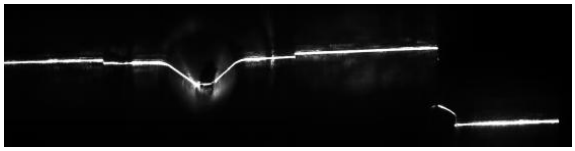

Fig. 10. The original image of laser light stripe.

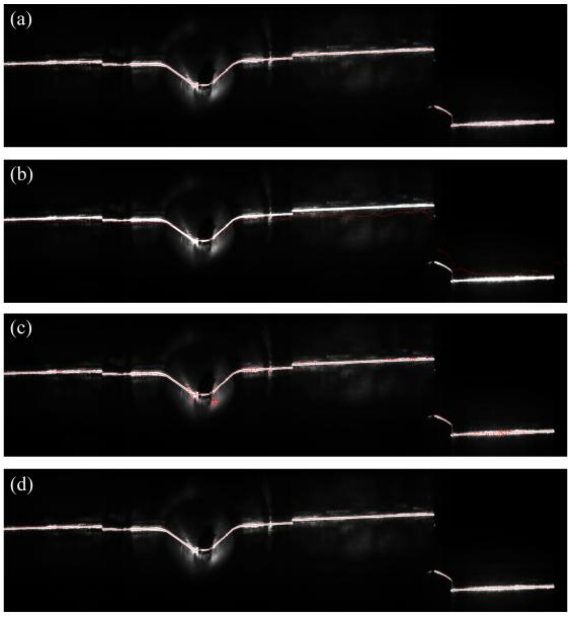

Fig. 11. Extraction results comparison of algorithms. (a) The Steger method; The gray-scale center of gravity method; (c) The thinning method; (d) The proposed method.

From the extraction result, the Steger method can preliminarily extract center points of the laser stripe. But since the the laser stripe does not conform to a perfect Gaussian distribution and is affected by the edge diffusion noise, this results in complex light intensity distributions near the edges. Such conditions can lead to erroneous extraction of multiple center points that erroneously incorporate noise points into the laser center line. The gray-scale center of gravity method calculates the centroid for the entire column, which causes failure in accurate center line extraction of laser stripe under image noise interference. The thinning method is similarly compromised by edge diffusion noise, leading to erroneous skeleton extraction from noise points. In contrast, the proposed method demonstrates noise immunity and precisely extracts a set of center points that align well with the shape of the laser stripe. Additionally, the center points are extracted with great continuity and smoothness. This is because the algorithm uses the candidate points mechanism and takes advantage of the DWMF-SC method for candidate points selection, which effectively avoids the influence of noise.

C. *Experiment of volume measurement*

To validate the effectiveness of the proposed CSBO method, we conducted comparative analyses using transparent adhesives specimens. First, the experimental setup employed a precision dispensing nozzle to extrude similar linear transparent adhesives beads onto four distinctive color (green-yellow, blue, pink, purple) background substrate, detailed in Fig. 12. Then the dispensed adhesives specimens were weighed using a precision electronic balance, with the measured mass systematically documented as reference true value. Experimental verification was performed using the previously described 3D line laser scanning system in a workshop environment to collect the surface data of the specimens. After that, the image processing module implemented 3D surface reconstruction and volume measurement of dispensed adhesives through a series of proposed algorithms. To minimize random variability, we performed repeated experimental trials on each specimen of distinct color substrate, followed by calculating 5 sets of dispensing transparent adhesives volume measurements from each specimen. Assuming the transparent adhesives density value is ρ and predicted volume value is V , the relative error ratio of volume measurement can be expressed mathematically as:

$$\delta = \frac{\Delta}{G_t} * 100\% \tag{12}$$

Here, $\Delta = G_t - G$ denotes absolute error of volume measurement, G_t represents the actual weight of dispensed adhesives, $G = V * \rho$is predicted weight of dispensed adhesives. The experimental results of each specimen volume measurement are shown in Tab. 2. For better visualization, the max and average relative error ratio of each specimen was transformed into the histogram shown in Fig. 13. From the table and histogram experimental data, we can see that the max and average error ratio of specimen 1 with green-yellow substrate is about 4 times lower than the others, which can reach about 1.40%. These results demonstrate that the CSBO method significantly enhances the 3D reconstruction accuracy of transparent adhesives.

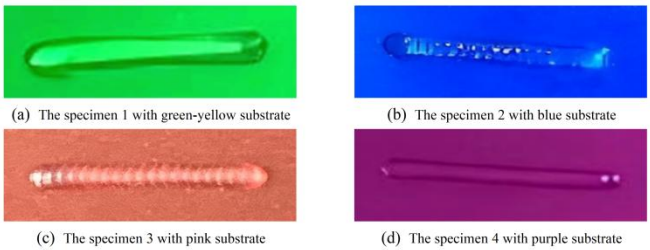

Fig. 12. The designed four different specimens.

TABLE II. VOLUME MEASUREMENT EXPERIMENTAL RESULT BETWEEN THE PROPOSED METHOD AND OTHER METHODS.

Test specimen	NUM	Volume (mm3)	Relative error (%)
Specimen 1 Green-yellow color ρ = 0.0011(g/mm3) G_t = 0.0145(g)	1	13.008193	1.32%
	2	13.007472	1.32%
	3	13.001968	1.36%
	4	12.994639	1.42%
	5	12.977638	1.55%
Specimen 2 Blue color ρ = 0.0011(g/mm3) G_t = 0.0124(g)	1	10.243669	9.13%
	2	10.283064	8.78%
	3	10.247479	9.10%
	4	10.246467	9.10%
	5	10.24006	9.16%
Specimen 3 Pink color ρ = 0.0011(g/mm3) G_t = 0.0152(g)	1	12.71021	8.02%
	2	12.7075	8.04%
	3	12.705905	8.05%
	4	12.708477	8.03%
	5	12.711013	8.01%
Specimen 4 Purple color ρ = 0.0011(g/mm3) G_t = 0.0108(g)	1	8.975904	8.58%
	2	8.97253	8.61%
	3	8.969407	8.65%
	4	8.965168	8.69%
	5	8.973207	8.61%

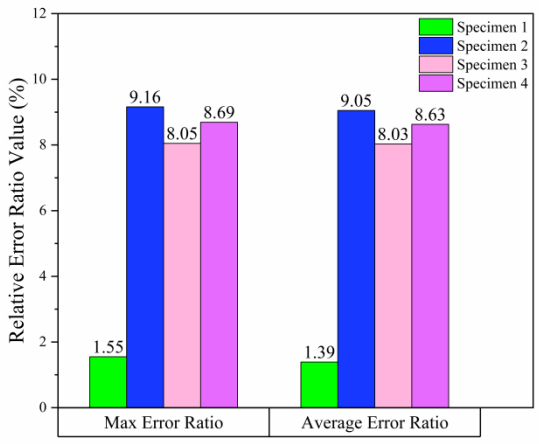

Fig. 13. Comparison of the max and average relative error ratio of each specimen.

VI. CONCLUSION

To address the limitations of pronounced measurement inaccuracy, time-consuming processes, substantial equipment costs in traditional measurement methods for calibration of transparent adhesives discharge, a new volume measurement system for transparent adhesives was designed based on line laser scanning technology. By utilizing a unique candidate points mechanism and the novel DWMF-SC method for candidate points screening, we leverage the advantage of multi-factor integrated assessment to develop an improved gray-scale center of gravity extraction algorithm. The proposed method can effectively mitigate judgmental errors caused by oversimplified single-variable evaluation while enhancing process stability and selection accuracy. To improve the 3D reconstruction accuracy of transparent adhesives, this paper proposes the CSBO method through the implementation of substrate with green-yellow spectral absorption characteristics. This approach attenuates the transmission light to suppress internal scattering and reflection interference without auxiliary measurement technologies and equipment, significantly reducing computational and hardware costs while enhancing 3D reconstruction effect for transparent adhesives.

Experimentally, laser center line extraction experiment was performed on the image with significant surface roughness and edge diffusion noise. The proposed method demonstrates more matching, continuous and smooth compared to the other traditional laser center line extraction methods. A volume measurement experiment was conducted to assess the efficacy of the proposed CSBO method. Compared with ground truth values, the proposed approach achieved the lowest relative error ratio reaching about 1.40%. This experimental measurement results fully prove that the CSBO method enhances the 3D reconstruction accuracy of transparent adhesives by attenuating the transmission light, which effectively suppresses internal scattering and reflection interference without requiring auxiliary measurement technologies or equipment.

Acknowledgment: This research is fully conducted and supported by OPT Machine Vision.

REFERENCES

[1] Q. Zhang, F. Liu, L. Lu, Z. Su, W. Pan, and X. Dai, “Reconstruction of transparent objects using phase shifting profilometry based on diffusion models,” Optics Express, vol. 32, No. 8, pp. 13342–13356, 2024.

[2] W. Pan, B. Jiang, W. Tang, F. Wu, and S. Li, “Gap measurement method based on projection lines and convex analysis of 3D points cloud,” Measurement Science and Technology, vol. 35, No. 10, p. 105024, 2024.

[3] A. Kume, “Importance of the green color, absorption gradient, and spectral absorption of chloroplasts for the radiative energy balance of leaves,” Journal of plant research, vol. 130, pp. 501–514, 2017.

[4] M. C. Beard, J. L. Blackburn, J. C. Johnson, and G. Rumbles, “Status and Prognosis of Future-Generation Photoconversion to Photovoltaics and Solar Fuels,” ACS Energy Letters, vol. 1, No. 2, pp. 344–347, 2016.

[5] Y. Huang, W. Kang, and Z. Lu, “Improved Structured Light Centerline Extraction Algorithm Based on Unilateral Tracing,” in Photonics, MDPI, 2024, p. 723.

[6] Y.-C. Fan, C. J. Huang, and C. M. Yelamandala, “Image Recognition Based on High Accuracy 3D Depth Map Information,” Journal of Advances in Information Technology, vol. 14, No. 5, pp. 1082–1087, 2023.

[7] J. Zhou, W. Jin, M. Wang, X. Liu, Z. Li, and Z. Liu, “Improvement of normal estimation for point clouds via simplifying surface fitting,” Computer-Aided Design, vol. 161, p. 103533, 2023.

[8] P. Marker, R. Jirasek, T. Schmidt, and A. Bleicher, “Development, realization, and experimental validation of an active hybrid roof structure based on elastic kinetic and rigid-body transformation,” International Journal of Space Structures, vol. 38, No. 2, pp. 83–100, 2023.

[9] Z. Yang and S. Farsiu, “Directional connectivity-based segmentation of medical images,” in Proceedings of the IEEE/CVF conference on computer vision and pattern recognition, 2023, pp. 11525–11535.

[10] J. Wang and X. Ren, “A consistent projection integration for Galerkin meshfree methods,” Computer Methods in Applied Mechanics and Engineering, vol. 414, p. 116143, 2023.